BATLAS: Deconvoluting Brown Adipose Tissue

Perdikari, Aliki ; Leparc, Germán Gastón ; Balaz, Miroslav ; Pires, Nuno D ; Lidell, Martin E ; Sun, Wenfei ; Fernandez-Albert, Francesc ; Müller, Sebastian ; Akchiche, Nassila ; Dong, Hua ; Balazova, Lucia ; Opitz, Lennart ; Röder, Eva ; et al ; Wolfrum, Christian

Abstract: Recruitment and activation of thermogenic adipocytes have received increasing attention as a strategy to improve systemic metabolic control. The analysis of brown and brite adipocytes is complicated by the complexity of adipose tissue biopsies. Here, we provide an in-depth analysis of pure brown, brite, and white adipocyte transcriptomes. By combining mouse and human transcriptome data, we identify a gene signature that can classify brown and white adipocytes in mice and men. Using a machine-learning-based cell deconvolution approach, we develop an algorithm proficient in calculating the brown adipocyte content in complex human and mouse biopsies. Applying this algorithm, we can show in a human weight loss study that brown adipose tissue (BAT) content is associated with energy expenditure and the propensity to lose weight. This online available tool can be used for in-depth characterization of complex adipose tissue samples and may support the development of therapeutic strategies to increase energy expenditure in humans.

DOI: https://doi.org/10.1016/j.celrep.2018.09.044

Resource

Cell Reports

BATLAS: Deconvoluting Brown Adipose Tissue

Graphical Abstract

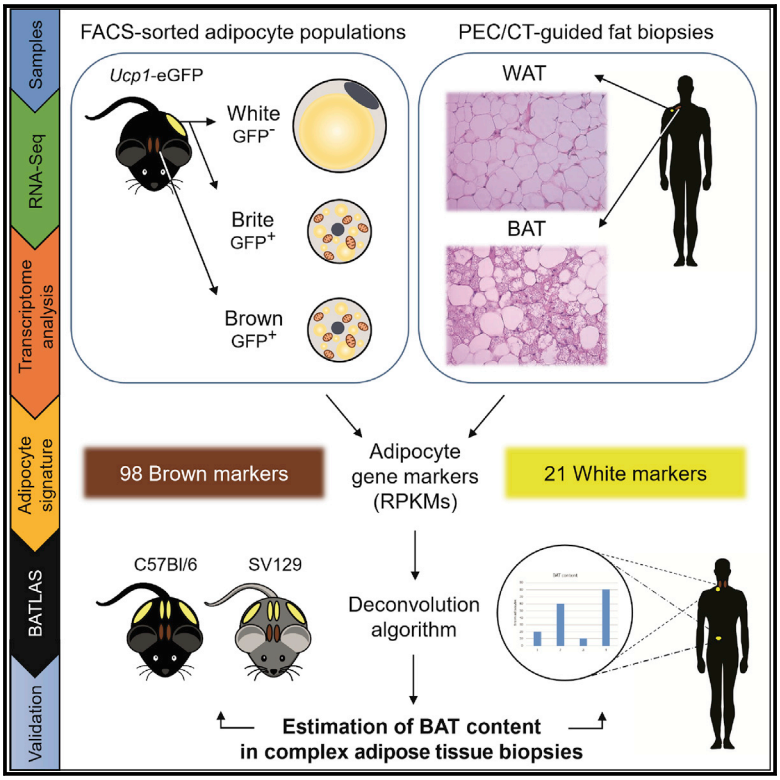

Highlights

- In-depth analysis of pure brown, brite, and white adipocyte transcriptomes
- Identification of a signature that can classify brown and white adipose depots
- BATLAS is a web tool that can be used to characterize complex fat tissues
- BATLAS can predict the brown adipocyte content in mixed populations of adipocytes

Authors

Aliki Perdikari, Germán Gastón Leparc, Miroslav Balaz, ..., Elia Stupka, Heike Neubauer, Christian Wolfrum

Correspondence

heike.neubauer@boehringer-ingelheim.com (H.N.), christian-wolfrum@ethz.ch (C.W.)

In Brief

By combining mouse and human transcriptome data, Perdikari et al. identify a gene signature that can classify brown and white adipocytes. Using a machine-learning-based cell deconvolution approach, they develop an algorithm proficient in calculating the brown adipocyte content in complex biopsies. This web tool allows in-depth characterization of adipose tissue samples.

Perdikari et al., 2018, Cell Reports *25*, 784–797
October 16, 2018
https://doi.org/10.1016/j.celrep.2018.09.044

CellPress

OPEN ACCESS
CellPress

Cell Reports
Resource

BATLAS: Deconvoluting Brown Adipose Tissue

Aliki Perdikari,[1,11] Germán Gastón Leparc,[2,11] Miroslav Balaz,[1,11] Nuno D. Pires,[1] Martin E. Lidell,[3] Wenfei Sun,[1] Francesc Fernandez-Albert,[2] Sebastian Müller,[1] Nassila Akchiche,[1] Hua Dong,[1] Lucia Balazova,[1] Lennart Opitz,[1] Eva Röder,[1] Holger Klein,[2] Patrik Stefanicka,[5] Lukas Varga,[5,6] Pirjo Nuutila,[4] Kirsi A. Virtanen,[4] Tarja Niemi,[8] Markku Taittonen,[9] Gottfried Rudofsky,[10] Jozef Ukropec,[6] Sven Enerbäck,[3] Elia Stupka,[2] Heike Neubauer,[7,*] and Christian Wolfrum[1,12,*]

[1]Institute of Food, Nutrition and Health, ETH Zurich, Schwerzenbach, Switzerland
[2]Target Discovery Research Department, Boehringer Ingelheim Pharma GmbH and Co. KG, Biberach/Riss, Germany
[3]Department of Medical and Clinical Genetics, Institute of Biomedicine, Sahlgrenska Academy, University of Gothenburg, Gothenburg, Sweden
[4]Turku PET Centre, University of Turku, Turku, Finland
[5]Department of Otorhinolaryngology – Head and Neck Surgery, Faculty of Medicine and University Hospital, Comenius University, Bratislava, Slovakia
[6]Institute of Experimental Endocrinology, Biomedical Research Center at the Slovak Academy of Sciences, Bratislava, Slovakia
[7]Cardiometabolic Diseases Research Department, Boehringer Ingelheim Pharma GmbH and Co. KG, Biberach/Riss, Germany
[8]Department of Surgery, Turku University Hospital, Turku, Finland
[9]Department of Anesthesiology, Turku University Hospital, Turku, Finland
[10]Endocrinology and Metabolic Diseases, Cantonal Hospital Olten, Olten, Switzerland
[11]These authors contributed equally
[12]Lead Contact
*Correspondence: heike.neubauer@boehringer-ingelheim.com (H.N.), christian-wolfrum@ethz.ch (C.W.)
https://doi.org/10.1016/j.celrep.2018.09.044

SUMMARY

Recruitment and activation of thermogenic adipocytes have received increasing attention as a strategy to improve systemic metabolic control. The analysis of brown and brite adipocytes is complicated by the complexity of adipose tissue biopsies. Here, we provide an in-depth analysis of pure brown, brite, and white adipocyte transcriptomes. By combining mouse and human transcriptome data, we identify a gene signature that can classify brown and white adipocytes in mice and men. Using a machine-learning-based cell deconvolution approach, we develop an algorithm proficient in calculating the brown adipocyte content in complex human and mouse biopsies. Applying this algorithm, we can show in a human weight loss study that brown adipose tissue (BAT) content is associated with energy expenditure and the propensity to lose weight. This online available tool can be used for in-depth characterization of complex adipose tissue samples and may support the development of therapeutic strategies to increase energy expenditure in humans.

INTRODUCTION

Two major types of adipocytes are found in mammals, namely white and brown adipocytes. White adipocytes are responsible for energy storage and consist mainly of a unilocular lipid droplet, and brown adipocytes are smaller, have a multilocular appearance, and express uncoupling protein 1 (UCP1), which conveys the ability for non-shivering thermogenesis, the main function of brown adipose tissue (BAT) (Cannon and Nedergaard, 2004). Apart from classical brown adipocytes, another type of thermogenic cell can be found interspersed in various white adipose tissue (WAT) depots after exposure to cold or β-adrenergic stimulation (Collins et al., 1997; Cousin et al., 1992; Guerra et al., 1998; Young et al., 1984). These so-called brite, beige, inducible, or brown-like adipocytes (Petrovic et al., 2010; Schulz et al., 2011; Waldén et al., 2012) show similar morphology and function (Giralt and Villarroya, 2013; Harms and Seale, 2013). Nevertheless, at least in mice, most of the thermogenic capacity is retained in BAT (Kalinovich et al., 2017). Even though several tracing studies have been performed, the origin of brite adipocytes remains elusive (Sanchez-Gurmaches and Guertin, 2014a). The interest for brown and brite adipocytes and their therapeutic potential has become more prominent after the discovery that BAT exists also in adult humans (Bartesaghi et al., 2015; Cypess et al., 2009; Frontini et al., 2013; van Marken Lichtenbelt et al., 2009; Virtanen et al., 2009), as activation of BAT leads to an increased energy expenditure and improvement of whole-body energy homeostasis (Broeders et al., 2015; Chen et al., 2013; Feldmann et al., 2009; Ouellet et al., 2012; Stanford et al., 2013). Furthermore, inverse relationships between presence and/or activity of BAT, BMI, and the metabolic syndrome have been reported (Carey et al., 2013; Cypess et al., 2015).

Several studies have investigated the characteristics of brown, brite, and white adipocytes and identified specific genes for these cell types, mainly in whole adipose tissue depots (de Jong et al., 2015; Harms and Seale, 2013; Shinoda et al., 2015; Waldén et al., 2012; Wang et al., 2016; Wu et al., 2012). Because brite adipocytes represent only ~2% of the total cells in the inguinal WAT (iWAT) depots (Rosenwald and Wolfrum, 2014), such an approach is problematic. Further characterization of

brite adipocytes has been based on *ex vivo* generated cells using stable clones derived from iWAT (Wu et al., 2012); however, as we have demonstrated that culturing changes the transcriptional profile of adipocyte precursors substantially (Schwalie et al., 2018), it is possible that the molecular signature of these cells might be altered. Here, we aimed to overcome these problems by isolating pure cell populations of brown, brite, and white adipocytes to identify their molecular signature. Using a combined bioinformatics analysis of murine brown and white adipocytes and human BAT and WAT transcriptomes, we were able to identify an adipocyte signature that can classify BAT and WAT depots and predict the brown adipocyte content in complex human and mouse biopsies.

RESULTS

Transcriptome Signatures of Murine Brown, Brite, and White Adipocytes

In order to analyze brown, brite, and white adipocyte transcriptomes, we isolated and characterized pure populations of the three cell types by RNA sequencing (RNA-seq). Therefore, transgenic *Ucp1-eGFP* mice, expressing the EGFP protein under the control of *Ucp1* promoter, were cold acclimated at 8°C for 7 days and the mature adipocyte fractions from interscapular BAT (iBAT) and iWAT were separated by fluorescence-activated cell sorting (FACS) (Figure 1A) using EGFP. We first defined the adipocyte population in the forward and side scatter by size and internal complexity characteristics. Subsequently, we defined the GFP^+ population in the respective gate and isolated the mature brown adipocytes from the iBAT mature fraction (Figure 1B). We employed the same strategy for the iWAT mature adipocyte fraction to isolate the GFP^+ population, which constitutes brite adipocytes, and the adjacent GFP^- population that constitutes white adipocytes (Figure 1B). Microscopic analysis of FACS-isolated brown, brite (GFP^+), and white adipocytes (GFP^-) demonstrated that cells are intact and have a multilocular and unilocular morphology (Figure 1C). Due to the isolation technique and the size of the nozzle, a bias toward smaller white adipocytes was observed. To confirm the nature and purity of the three different adipocyte populations, we quantified the expression of the brown adipocyte marker *Ucp1* and the general adipocyte marker peroxisome proliferator activator γ (*Ppar*γ) (Figure 1D). We could confirm that *Ucp1* expression was restricted to isolated mature brown and brite adipocyte populations and that *Ppar*γ was expressed at equal levels in all FACS-isolated populations. Similar to *Ucp1*, other brown adipocyte markers, such as cell death activator (*Cidea*) and cytochrome C oxidase subunit VIIa polypeptide 1 (*Cox7a1*), were highly expressed in brown and brite adipocyte populations (Figure 1D) and absent or expressed at much lower levels in white adipocyte populations.

To assess the expression profiles of these populations, we sequenced RNA extracted from FACS-isolated mature brown, brite, and white adipocytes. A principal-component analysis (PCA) combining all RNA-seq data after batch effect removal revealed that brown and brite adipocytes clustered together and were clearly separated from white adipocytes (PC1) (Figures 1E, S1A, and S1B). In PC2, there is a gradation of brite to brown adipocyte samples with an overlap of 16% (8 out of 50) between the two groups. Furthermore, in PC3, the separation becomes slightly greater between the brown adipocytes and the rest of the adipocytes, as can be seen in the upper-left quadrant (Figures S1A and S1B). These differential gene expression analyses suggest that, although brown and brite adipocytes have a similar transcriptional profile, nevertheless, some intrinsic differences can be found between these two cell types. We identified 322 differentially expressed genes (DEGs) between brown and brite adipocytes, 4,491 DEGs between brown and white adipocytes, and 3,293 DEGs between brite and white adipocytes at false discovery rate (FDR) ≤ 0.05 and log2 fold change ≥ 0.5 (Table S1). As expected, the isolated mature brown and brite adipocytes expressed "classical" brown adipocyte markers, such as *Ucp1*, *Cidea*, iodothyronine deiodinase 2 (*Dio2*), glycerol kinase (*Gyk*), adenylate cyclase 3 (*Adcy3*), and *Cox7a1*. Moreover, brown adipocytes retained the expression of markers proposed in literature as "brown" specific, such as zic family member 1 (*Zic1*) (Timmons et al., 2007), homeobox a2 (*Hoxa2*) (Lim et al., 2016), early B cell factor 2 (*Ebf2*) (Wang et al., 2014), solute carrier family 29 member 1 (*Slc29a1*) (Wu et al., 2012), and bone morphogenic protein 8b (*Bmp8b*) (Whittle et al., 2012), and brite adipocytes expressed several "brite"-specific markers, among them homeobox C9 (*Hoxc9*) (Waldén et al., 2012), solute carrier family 27 member 1 (*Slc27a1*), T-box 1 (*Tbx1*) (Wu et al., 2012), and short stature homeobox 2 (*Shox2*) (Waldén et al., 2012; Table S1). In-depth analysis of the 322 DEGs between brown and brite adipocytes showed that 71 of these genes were not differentially expressed between brown and white adipocytes, suggesting that they might be considered as general adipocyte markers. Interestingly, *Hoxc9* and *Shox2* were also highly expressed in white adipocytes of inguinal WAT, and a similar pattern of expression was observed for 133 other genes, suggesting that these might constitute depot-specific, rather than brite-specific, markers. Using the identified DEGs in an ingenuity pathway analysis, we could show that brown and brite adipocyte comparison identified the methylglyoxal degradation III pathway as the most highly regulated, followed by the acute phase response system and the oxidative phosphorylation pathway. Interestingly, analysis of the comparison between brown or brite adipocytes with white adipocytes showed that the main regulated pathways in both comparisons are linked to oxidative phosphorylation and mitochondrial dysfunction, followed by tricarboxylic acid (TCA) cycle II and endothelin 1 signaling, suggesting that the main feature of brown and brite cells, namely energy metabolism, is shared between the two cell types.

Transcriptome Analysis of Human BAT and WAT Reveals Different Nature of the Two Fat Depots

The main aim of the current study was to identify a common signature of brown and brite adipocytes between mice and humans, which can be used to predict the content of cells having the potential of thermogenesis upon activation in complex human biopsies. The origin of human brown adipocytes is not yet fully understood, because it is problematic to obtain human biopsies, and any comparison made with markers identified in mice propose that these cells are either similar to murine brite adipocytes (Sharp et al., 2012; Wu et al., 2012) or to classical

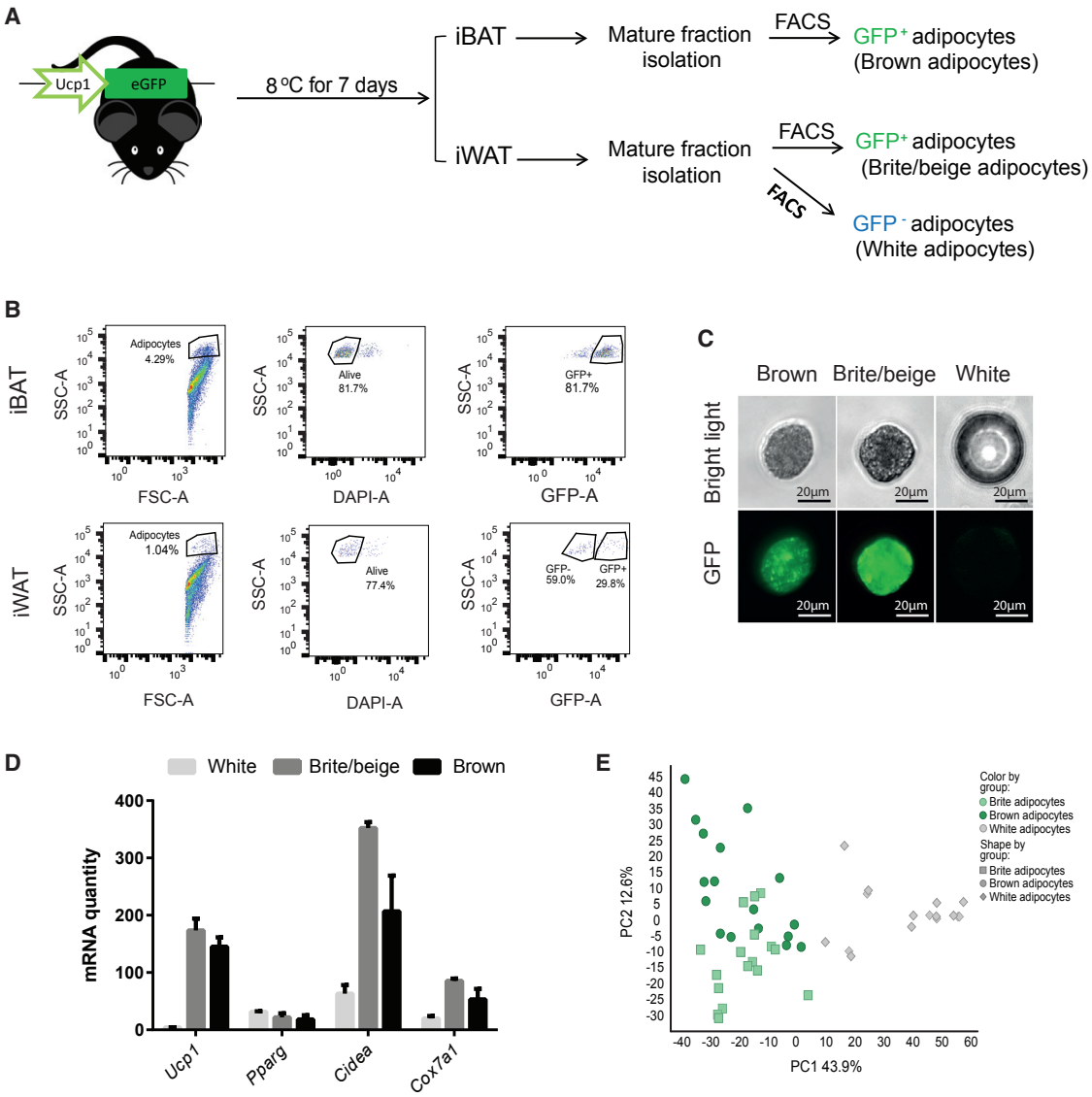

Figure 1. Isolation of Mouse Mature Brown, Brite, and White Adipocyte Populations by FACS and Comparison of Transcriptomes

(A) Workflow for isolation of mature adipocyte populations by FACS.

(B) Representative FACS plots from interscapular BAT (iBAT) and inguinal WAT (iWAT) and gating strategy for GFP$^+$ brown adipocytes, GFP$^+$ brite adipocytes, and GFP$^-$ white adipocytes.

(C) Representative microscopic pictures of mature brown, brite, and white adipocytes after FACS. Top panels: bright field is shown; bottom panels: GFP channel is shown.

(D) mRNA expression levels of brown-adipocyte-specific genes (*Ucp1*, *Cidea*, and *Cox7a1*) and adipocyte marker *Pparγ* in isolated mature brown, brite, and white adipocytes. n = 3; mean ± SD.

(E) Separation of samples from RNA-seq of mouse mature brown, brite, and white adipocytes (n = 17) by principal-component analysis (PCA).

murine brown adipocytes, depending on the depot and the depth of the biopsy (Cypess et al., 2013; Jespersen et al., 2013; Lidell et al., 2013). To expand our studies to the human system, we obtained BAT and WAT samples from two different human cohorts and analyzed their transcriptome by RNA-seq. The first set of samples was obtained by positron emission tomography (PET)/computed tomography (CT) scan-guided biopsies from the supraclavicular region (Orava et al., 2011). Patients were subjected to PET-CT upon cold exposure in order to identify areas showing high ^{18}FDG uptake, which represent functional BAT (Figure 2A). Guided by the PET-CT scans, BAT biopsies were taken from the supraclavicular region after return of the patients to normal temperature. From each subject, a subcutaneous WAT biopsy was taken from the same incision as the BAT (cohort 1). Paired transcriptome analysis of all 7 patients showed that most of the supraclavicular BAT biopsies can be

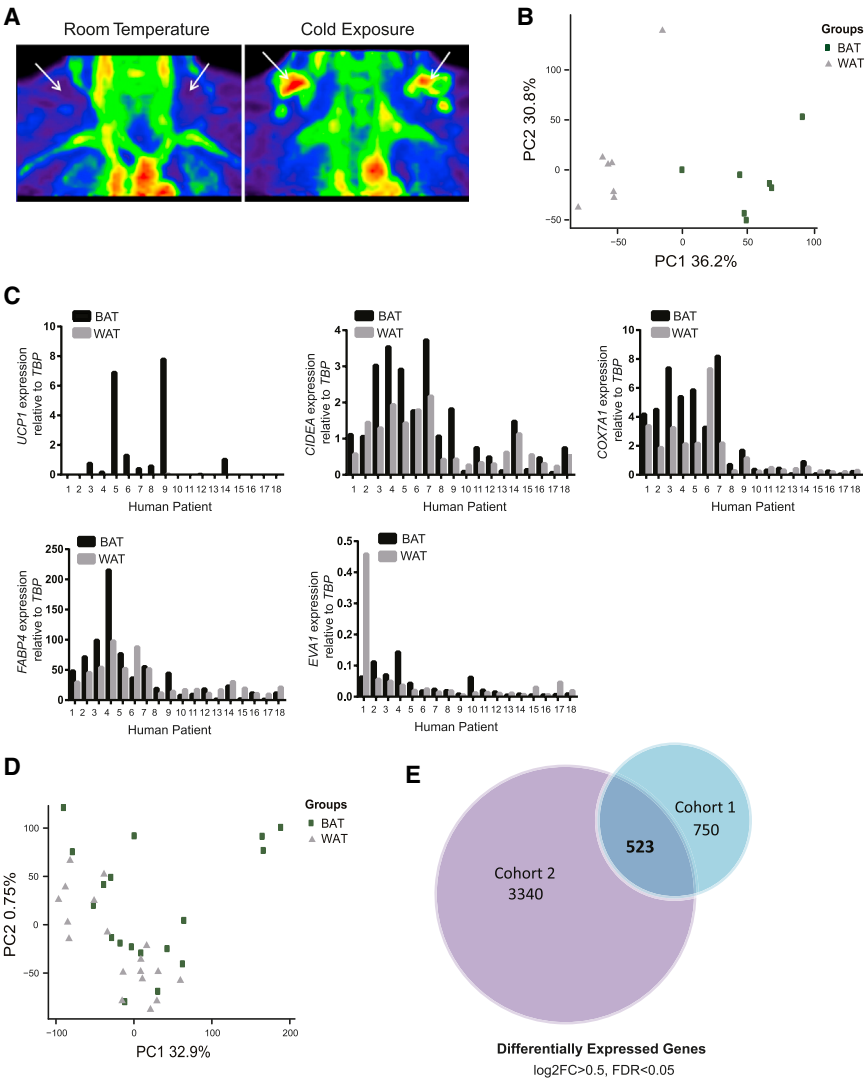

Figure 2. Transcriptome Analysis of Human BAT and WAT Samples from Supraclavicular BAT and Subcutaneous WAT (Cohort 1) and Deep Neck BAT and Subcutaneous WAT (Cohort 2)

(A) Representative PET images of human patients from cohort 1 at room temperature and under cold exposure.

(B) Separation of samples from RNA-seq of cohort 1 by PCA (n = 7 per group).

(C) mRNA expression of brown adipocyte marker genes from cohort 2 in BAT and WAT samples (n = 18).

(D) Separation of samples from RNA-seq of cohort 2 by PCA (n = 18).

(E) Venn diagram depicting differentially expressed genes from paired analysis of cohort 1 and cohort 2 and the overlap between the two studies.

clearly separated from the subcutaneous WAT biopsies on a transcriptome level (Figure 2B), and differential gene expression analysis revealed 1,273 DEGs between BAT and WAT samples (Table S2). In the second approach, deep neck BAT and subcutaneous WAT biopsies were obtained from patients undergoing partial excision of thyroid gland or lateral cervical cyst based on the morphological characteristics of the tissue (cohort 2; Müller et al., 2016). To identify whether a deep neck biopsy contained BAT, expression levels of different brown adipocyte markers were analyzed (Figure 2C). Interestingly, using this approach, BAT and WAT samples from cohort 2 could not be fully separated in the PCA, even though in some of the biopsies *UCP1* expression showed strong differences (Figures 2C and 2D). Transcriptomic analysis of the biopsies obtained from cohort 2 led to the identification of 3,868 DEGs (Table S3). Interestingly, in both human transcriptome analyses, we identified a higher number of DEGs than in the pure mouse adipocyte analysis. We assume that this discrepancy in the DEGs numbers is mainly due to sample composition, because in mice, we analyzed pure populations, and the human analyses were performed on whole-tissue biopsies. Comparison of the DEGs between cohorts 1 and 2 revealed 523 DEGs commonly regulated between BAT and WAT (Figure 2E). The fact that cohort 1 showed less DEGs in comparison to cohort 2 and that their overlap is rather small, depicts mainly the differences in the collection procedure and especially the sample purity. Given the fact that future studies will aim at analyzing large sample sizes, PET-CT-guided sample preparation is problematic and probably not feasible. Therefore, it is important to develop bioinformatics tools to analyze more complex samples from regular surgical procedures.

In summary, a paired transcriptome analysis of BAT and WAT from two different human cohorts led to the identification of a large number of genes that characterize these two functionally and morphologically distinct tissues. Furthermore, the comparison of different technical approaches to obtain human material clearly underlines the difficulties in obtaining clean representative tissue biopsies.

Gene Signature for Brown and White Adipocytes Obtained by Combining Mouse and Human Transcriptomes

Obtaining biopsies of human BAT in order to perform downstream analyses and characterize this tissue in depth is complicated by the fact that adipose tissue in specific regions contains only small amounts of brown adipocytes. Therefore, we utilized the fact that our mouse transcriptome analysis is based on pure brown and brite adipocytes and combined these data with our human transcriptome analyses of BAT and WAT, with the aim to identify a brown or white adipocyte signature that

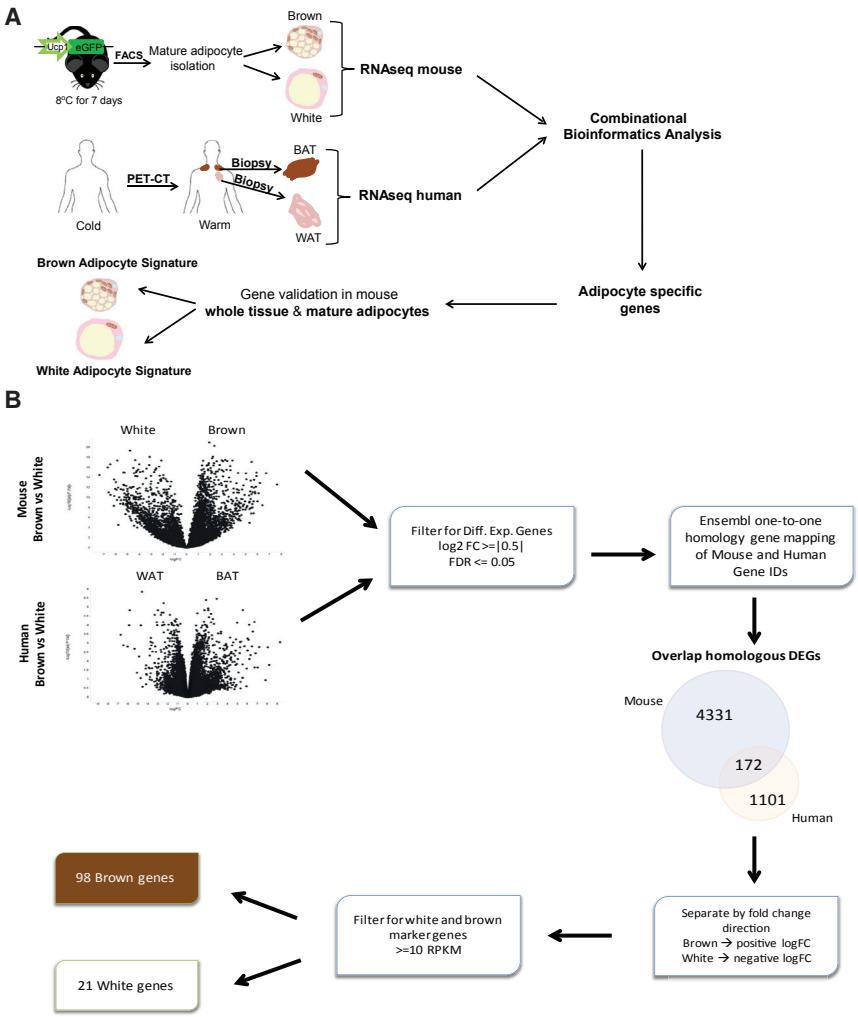

Figure 3. Combined Bioinformatics Analysis of Mouse Brown and White Adipocytes and Human BAT and WAT Transcriptomes Reveals a Common Signature for Brown and White Adipocytes

(A) Workflow for mouse and human combined bioinformatics analysis.

(B) Workflow for gene candidate selection.

Classification of BAT and WAT Depots through Gene Signature and Deconvolution of Brown Adipocyte Percentage in Whole Human Adipose Tissue Depots

In order to identify a gene list that can separate human biopsies into BAT and WAT and define the proportion of brown adipocytes in each biopsy, we used the gene signature identified by our mouse and human combined analysis (Table 1). To assess the individual quality of predictive value, we first investigated the performance of each individual gene in its ability to classify samples from the training set of FACS-isolated mature adipocyte populations into brown and white adipocytes. We analyzed their receiving operating characteristics (ROCs) curves and calculated the area under the curve (AUC) for each gene separately (Figure 4A; Data S1A). Because several markers have been reported in the literature as brown specific from mouse and human studies, we also analyzed their ability to classify samples from the FACS-isolated mature adipocyte populations (Table S4; de Jong et al., 2015; Sharp et al., 2012; Shinoda et al., 2015; Waldén et al., 2012; Wu et al., 2012). Interestingly, *UCP1* was the only gene that appeared in both lists (Tables 1 and S4). We could show that most of the genes in our list perform significantly better in comparison to the published genes (Figure 4A). In a next step, we applied the same analysis to the training set of human BAT and WAT samples from cohort 1, which once again showed the robustness of each individual gene from our list to separate the two tissues (Figure 4B; Data S1B). In addition to the evaluation of individual genes as classifiers, we also applied a support vector machine learning approach using all the 119 genes of our list. Two support vector classification (SVC) models using a radial kernel were fitted separately for human and mouse datasets (Fan et al., 2008) using the approach described in the STAR Methods section. The cross-validation accuracy rates showed good prediction for both mouse (Figure 4C; mean accuracy for 20-fold cross-validation = 96.5%) and human datasets (Figure S3A; mean accuracy for 20-fold cross-validation = 88.0%), further supporting the accuracy of our gene marker list. Although each gene has the potential to classify the clean FACS-isolated

could be applied to both human and mouse tissues (Figures 3A and S2A). We first analyzed overlapping DEGs from the RNA-seq analysis of mature murine brown, brite, and white adipocytes and human BAT and WAT from cohort 1, which resemble the most "pure" populations (Figure 3B). After filtering for high-confidence one-to-one mapping between human-mouse orthologs, we found an overlap of 172 DEGs between human and mouse datasets. This relatively limited number of overlapping genes is most likely due to the fact that the human and mouse are genetically different, resulting in gene expression differences between tissues (Lin et al., 2014). Moreover, different sample composition, whole adipose tissue from humans and pure adipocyte populations from mice, as well as the different RNA-seq techniques, lead to a smaller number of commonly expressed DEGs between human and mice. We further filtered these DEG orthologs for robustly expressed genes with read per kilobase per million (RPKM) values $\geq$10 and obtained a list of 119 genes that are differentially expressed and can serve as "bona fide" markers for either brown or white adipocytes both in mice and human (Figure 3B; Table 1).

Table 1. Gene Candidates for the Classification and Brown Adipocyte Proportion Estimation of BAT and WAT

ACADS
ACADVL
ACAT1
ACO2
ACSF2
ACSL5
ACVR1C
ADCY3
AGPAT3
AKAP1
AMACR
AURKAIP1
BCKDHB
BSG
C1QBP
CCDC80
CCND2
CHCHD3
CIAPIN1
COL3A1
COL4A2
COQ6
COX10
COX5A
COX7A2
CPT1B
CRLS1
CYC1
DES
DLD
DLST
DMRT2
DNAJA3
DNAJC11
ECH1
ECHS1
ECSIT
EEF2K
EEPD1
EHHADH
ETFA
FLAD1
GADD45A
GATB
GK
GLRX5
GOT1
HADHA
HCCS
HSPA9
HSPD1
IDH3A
IDH3B
IGF1
IMMT
KCNK3
LEP
LETMD1
LPGAT1
LRP1
MARCH5
MRPL15
MRPL34
MRPS18B
MRPS22
MRPS5
MRPS7
MT-CO3
MT-ND2
MT-ND3
MTIF2
NDRG1
NDUFA13
NDUFAB1
NDUFAF5
NDUFB2
NDUFB7
NDUFB9
NDUFS1
NDUFS2
NDUFS3
NDUFS8
NDUFV1
NNAT
NRIP1
NUPR1
OGDH
OXNAD1
PANK1
PCK1
PDHA1
PHB2
PIK3R1
POLDIP2
POLN
PPARGC1B
PPIF
PRKCDBP

(Continued on next page)

Table 1. *Continued*

PTCD3
PYGB
QSOX1
SDC4
SDHA
SDHC
SGPL1
SLC25A11
SLC25A39
SOD2
SUCLG1
TBRG4
THEM4
TIMM44
TIMM50
UCP1
UQCC1
UQCR10
UQCRB
UQCRC1
VWA8

mature adipocytes and the relatively clean human biopsies into brown and white, the same was not possible for heterogeneous populations. Therefore, in order to classify heterogeneous samples of adipose tissue in mice and humans and to estimate the brown adipocyte content in those samples, a gene signature will be more robust than individual genes.

To identify such a gene signature that can predict the proportion of brown adipocytes in a mouse and human heterogeneous adipose tissue, we performed a deconvolution analysis using the CellMix package (Gaujoux and Seoighe, 2013). To evaluate the performance of these algorithms, different *in silico* and *in vitro* test sets were analyzed. For each set, the 119 genes included in the gene list (Table 1) and their gene expression RPKM values were used as input. The estimated brown adipocyte proportions per sample from the deconvolution algorithms were evaluated against predetermined admixture proportions of brown to white using the root mean squared error (RMSE). As a comparison, we analyzed the Pearson correlation coefficient of *UCP1* expression in the respective datasets because *UCP1* is considered a unique marker for brown adipocytes. As a control, we first generated and analyzed an *in silico* test set by combining different proportions of RNA-seq reads from a pure brown adipocyte sample with a pure white adipocyte sample in varying ratios, in order to cover the full spectrum of brown percentages. In the analysis of the *in silico* test set, both the digital sorting algorithm (DSA) (Figure 5A) and the semi-supervised non-negative matrix factorization (NMF) algorithm for Kullback-Leibler divergence (ssKL) (Figure S4A) algorithms performed the best. We then analyzed a validation set comprised of samples from whole mature adipocyte fractions of iBAT, iWAT, and epididymal WAT (eWAT) from C57BL/6 and SV129 mice, fractions of which consist of different cell types, among them mature adipocytes. Using the CellMix package together with our gene list, we were able to estimate brown adipocyte proportions in each of the samples with the DSA and ssKL algorithms. The estimated proportions were compared with actual brown adipocyte proportions, as determined by quantifying the amount of brown adipocytes in tissue samples from iWAT of C57BL/6 and SV129 mice, together with an equation formed by expression data from the actual RNA-seq samples. Although both algorithms successfully predicted the brown adipocyte content in the mature adipocyte fractions, the DSA approach was determined to be more accurate and robust (Figures 5B and S4B).

The last step in our analysis involved the validation set of human BAT and WAT samples from cohort 2, in order to predict the brown adipocyte proportions in the context of the heterogeneous human adipose tissue. By implementing the DSA algorithm and our gene list used in the test sets in the validation set, we were able to successfully estimate the brown adipocyte content in each sample, compared to the actual brown adipocyte proportions of each human BAT sample as measured by microscopic analysis of paraffin sections, and quantification of multilocular cells (Figure 5C). The ssKL algorithm once again could not robustly estimate the brown adipocyte proportions in our validation dataset, suggesting that the DSA algorithm together with the 119-gene list is a useful tool when estimating brown adipocyte content in mouse and human heterogeneous adipocyte populations (Figure S4C). Comparing the results from the DSA algorithm and our 119 genes used with the *UCP1* expression correlation analysis, we could show that, even though there is a strong correlation between *UCP1* and brown adipocyte content in the *in silico* dataset and the C57BL/6 and SV129 mature adipocyte fraction datasets, the correlation is moderate when analyzing the deep neck human BAT (Figures 5A–5C). This suggests that, even though *UCP1* is a specific marker for brown adipocytes, it cannot be used to estimate BAT content in heterogeneous populations, such as human whole adipose tissue, without the presence of active BAT. Apart from *UCP1*, several other genes resulting from *in vitro* experiments were proposed as brown- and brite-adipocyte-specific markers that characterize human BAT tissue (Cypess et al., 2013; Shinoda et al., 2015), and their expression correlation with the deep neck BAT samples is presented in Table S5. Comparison of the literature human brown- and brite-adipocyte-specific markers with our gene list revealed 14 common genes, and from these, only PHB2 showed a negative R (Table S5). It is important to underline the fact that, with our algorithm, we did not only use brown but also white adipocyte markers, in order to be able to estimate brown adipocyte content in the basal state. In fact, several brown adipocyte markers, among them *UCP1*, might be highly expressed in the activated rather than in the basal state, suggesting that using a signature that includes only brown adipocyte markers might be relevant only to activated adipose tissue.

Brown Adipocyte Content in Subcutaneous WAT Increases after Caloric Restriction and Associates with Weight Loss and Energy Expenditure

To test whether our algorithm can be applied to answer burning questions in the brown adipocyte field, we calculated the content

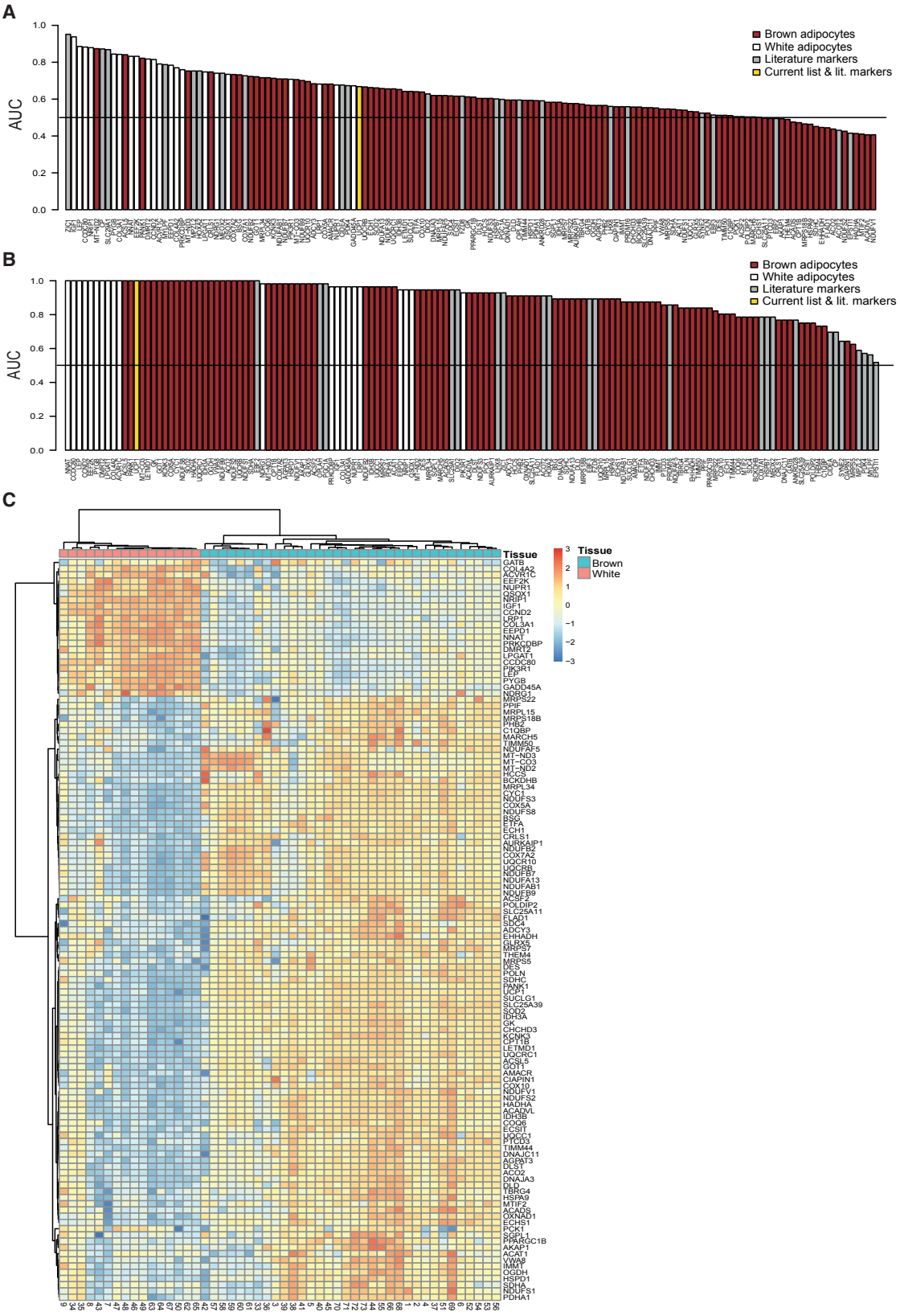

(legend on next page)

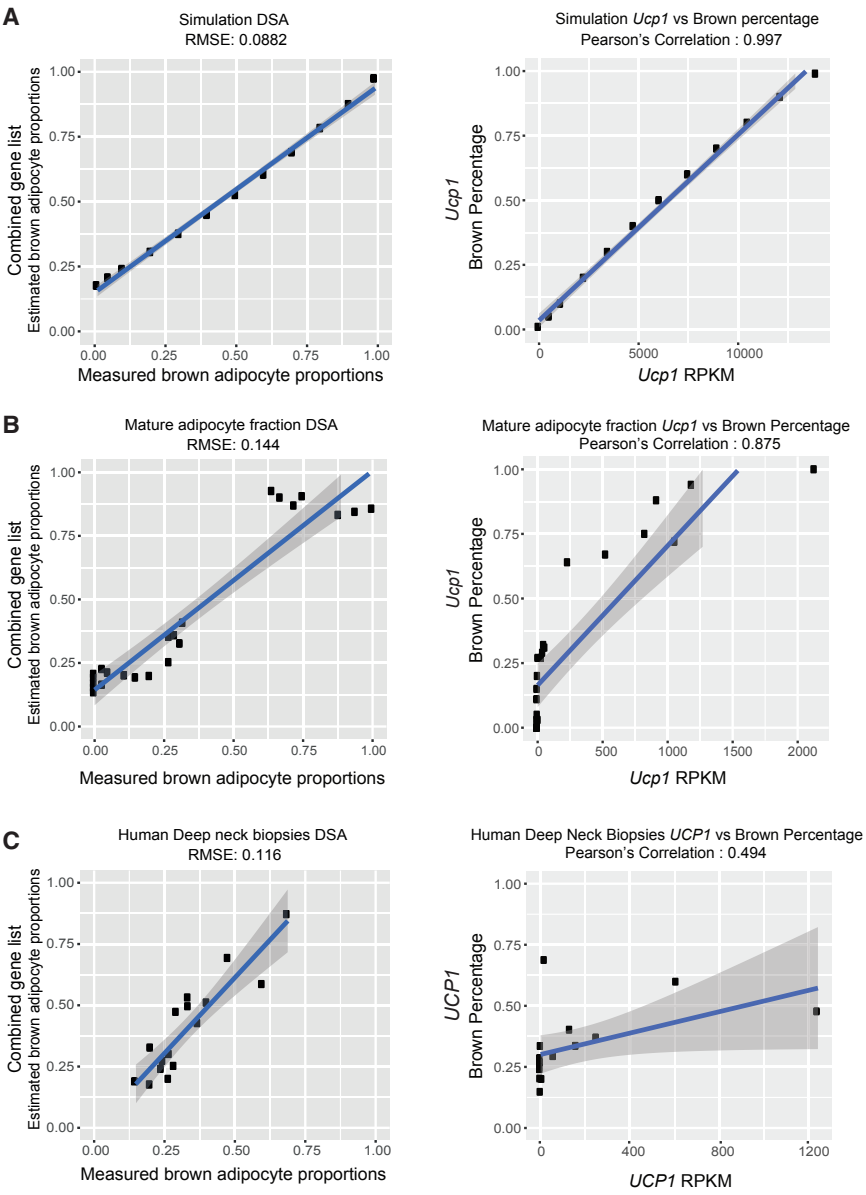

Figure 5. Deconvolution of Brown Adipocyte Percentage in Whole Human Adipose Tissue Depots

(A) Estimated brown adipocyte proportions for an *in silico* test set obtained by combination of different proportions of mouse brown and white adipocytes calculated by the DSA algorithm and using the 119 genes of the mouse and human combined gene list. The DSA algorithm performance is compared to the Pearson's correlation coefficient of *Ucp1* expression in the dataset.

(B) Estimated brown adipocyte proportions for the validation set of mature adipocyte fractions from interscapular BAT, inguinal WAT, and epididymal WAT of C57BL/6 and SV129 mice calculated by the DSA algorithm and using the 119 genes of the mouse and human combined gene list. The DSA algorithm performance is compared to the Pearson's correlation coefficient of *Ucp1* expression in the dataset.

(C) Estimated brown adipocyte proportions for the validation set of human BAT and WAT tissues from cohort 2 calculated by the DSA algorithm and using the 119 genes of the mouse and human combined gene list. The DSA algorithm performance is compared to the Pearson correlation coefficient of *UCP1* expression in the dataset. For association of BAT content with *UCP1* expression, Pearson's correlation coefficient was calculated and is shown in the figures.

of brown adipocytes in abdominal subcutaneous WAT biopsies of obese patients (20/42 male/female; age 40.5 ± 1.6 years; BMI 41.2 ± 0.9 kg/m^2) taken before as well as after 12 weeks of caloric restriction to assess the relevance of BAT for metabolism. Caloric restriction led to a 16.5% reduction in body weight (Figure 6A) and BMI (Figure S5A), which was mainly due to the reduction of fat mass (−12.2%; Figure 6B). The profound body weight loss led to a significant improvement of fasting blood insulin, cholesterol, and glucose levels (Figures S5B–S5D). Interestingly, by applying our algorithm to the transcriptome of abdominal subcutaneous WAT samples, we could show a 9% increase in brown adipocyte content after weight loss (Figure 6C). Similarly, expression of known brown adipocyte marker genes *UCP1* and *CIDEA* significantly increased by 31.5% and 16.7%, respectively (Figures 6D and 6E). BAT content, assessed using our algorithm, was positively correlated with weight loss (Figure 6F) and negatively with percentage of body fat (Figure 6G), BMI, and circulating levels of insulin and cholesterol (Figures S5E–S5G). Importantly, we found a strong positive correlation between brown adipocyte content and resting energy expenditure (Figure 6H). Stepwise multiple regression analysis revealed that BMI ($t = -3.17$; $p = 0.0031$), circulating cholesterol ($t = -3.01$; $p = 0.0047$), resting energy expenditure ($t = 2.76$; $p = 0.009$), and fat mass ($t = 2.26$; $p = 0.0297$) are the best predictors of BAT content, collectively

Figure 4. Evaluation of Gene Markers for Classification and Deconvolution of Brown and White Adipose Tissue Samples

(A and B) Ranking of individual gene markers in descending order based on the AUC of the ROC curve depicting performance for classification of (A) mature mouse adipocyte populations by FACS and (B) human supraclavicular BAT and subcutaneous WAT samples (cohort 1). The horizontal solid black line represents the no-discrimination line at 0.5 AUC.

(C) Heatmap depicting the RPKM gene expression values across mouse datasets on a log 10 scale for the 119 genes used as features in the support vector machine classifier. Genes are clustered by expression using the complete linkage method for hierarchical clustering from heatmap R package.

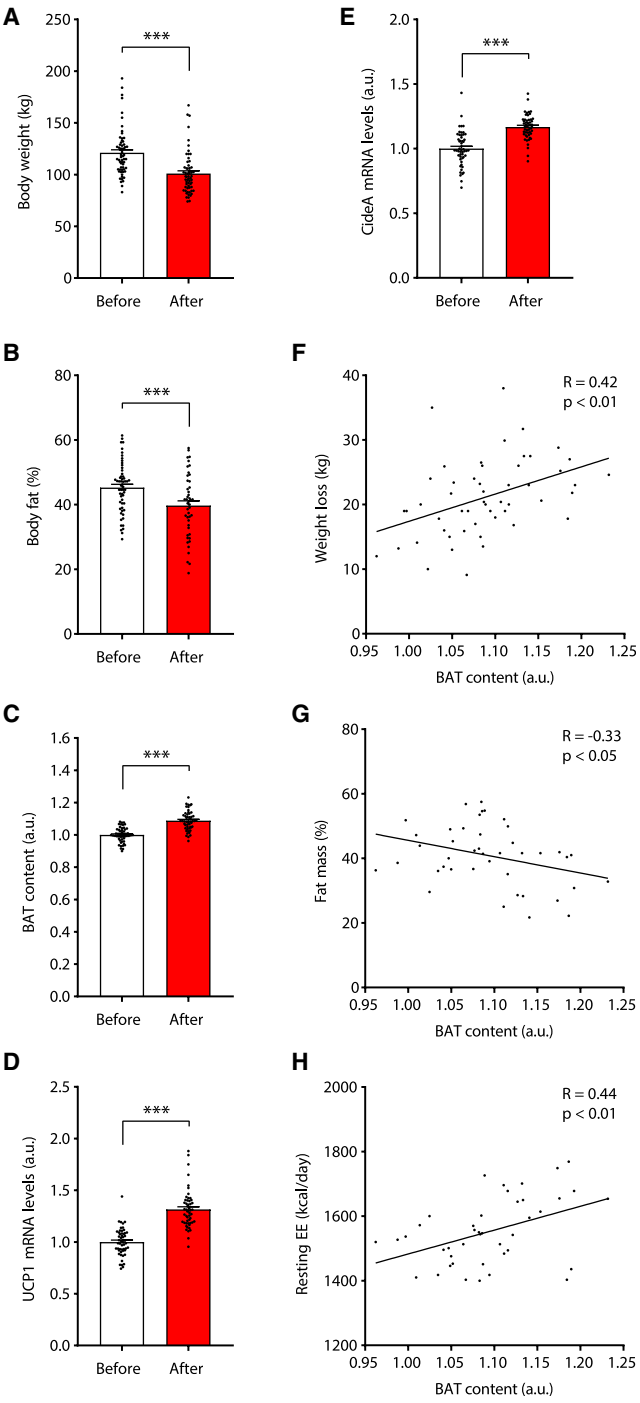

Figure 6. Caloric Restriction Increases Brown Adipocyte Content in Abdominal Subcutaneous WAT of Obese Patients

(A and B) Caloric restriction led to a significant reduction in (A) body weight (n = 60) and (B) fat mass (n = 46) in obese patients.

(C) BAT content in abdominal subcutaneous WAT, assessed using our deconvolution tool, increased following caloric restriction (n = 52).

(D and E) Caloric restriction led to a significant increase in (D) *UCP1* and (E) *CIDEA* gene expression (n = 52).

(F–H) BAT content in abdominal subcutaneous WAT is associated with (F) body weight loss, (G) fat mass, and (H) resting energy expenditure (n = 52).

explaining 43.7% of its variability ($R^2 = 0.437$; $F = 7.18$; $p < 0.001$; details in Table S6). Even though *UCP1* and *CIDEA* mRNA levels in abdominal subcutaneous WAT were also significantly increased following caloric restriction (Figures 6D and 6E), expression of these two genes alone was not related to any of the measured parameters (Figures S5H–S5L).

DISCUSSION

Several studies based on different approaches that focus on molecular markers for brown, brite, and white adipocytes and the genetic signature of these cell types have been published so far (Cypess et al., 2013; de Jong et al., 2015; Jespersen et al., 2013; Sharp et al., 2012; Shinoda et al., 2015; Waldén et al., 2012; Wang et al., 2016; Wu et al., 2012). The genetic marker analyses in humans were performed by applying the previous molecular markers from mice in human whole BAT and were also combined with *in vitro* analyses (Cypess et al., 2013; Jespersen et al., 2013). These different approaches have provided valuable information regarding brown, brite, and white adipocytes; however, due to the fact that most studies focus on either the mouse or the human system, a common molecular signature of the three different cell types in mice and humans is still not established. Furthermore, because BAT and WAT depots are highly heterogeneous, as they contain different cell types in different ratios (Lee et al., 2014; Rosenwald et al., 2013b), an extrapolation of the cell signature from whole tissue might in part reflect the tissue composition and thus mask changes in cell-specific gene expression. Moreover, the different mouse strains used for the analyses, the different experimental conditions, and the long experimental times for the *in vitro* culture experiments together with differences in cell culture techniques might cause discrepancies in the signature observed among the studies. In this context, recent studies from *ex vivo* isolated adipocytes from mice or humans have shed some further light into the nature of brown, brite, and white adipocytes and have shown the importance of using isolated cells in order to study the transcriptome of adipocytes in mice and human (Shinoda et al., 2015; Wang et al., 2016).

In our current study, we aimed first at isolating pure murine populations of brown, brite, and white adipocytes by FACS and analyzing their transcriptomes. Although the pure population of murine white adipocytes is biased toward smaller sized adipocytes due to the FACS isolation limitations, the white genes used in our signature retain their predictive power, as demonstrated by their use on the human samples, which consist of adipocytes with varying sizes. Nevertheless, it might be possible to enhance the predictive capacity by other transcript markers, which would be enriched in larger white adipocytes.

The fact that there are only 322 DEGs between brown and brite adipocytes suggests a great similarity of these two cell types on a transcriptome level. Our finding is further supported by a recent

Results are reported as mean ± SEM. Statistical significance for comparison of two groups was calculated using paired Student's t test. For association of BAT content with body weight loss, fat mass, and resting energy expenditure, Pearson's correlation coefficient was calculated. Statistical differences are indicated as ***$p < 0.001$.

study analyzing also FACS isolated adipocytes from mice upon injection with the β3-AR agonist CL316,243 (Wang et al., 2016). Further analysis will be required to understand whether the differences in gene expression between brown and brite adipocytes are attributed to a different developmental origin or location (Sanchez-Gurmaches and Guertin, 2014b) or an actual difference in their function and thermogenic capacity.

Predicting brown and brite adipocyte content in human biopsies is of great importance to correctly interpret the results from human BAT studies, which are currently based mainly on PET-CT scans, to understand the metabolic contribution of BAT and how it can regulate whole-body metabolism in health and disease. This necessity is exemplified by a recent study in which the authors mapped human BAT in lean and obese individuals to construct a human ''BATlas'' using a refined ^{18}FDG-PET-CT scan analysis (Leitner et al., 2017). The authors successfully localized BAT in the human body and were able to define the potential of each depot to accommodate thermogenic cells. However, even though it was possible to measure total BAT volume, the localized BAT remains a mixture of brown and white cells with unknown proportions. Thus, an ^{18}FDG-PET-CT scan only depicts active brown adipocytes and is not able to distinguish between the thermogenic and non-thermogenic cells, which precludes the calculation of the potential thermogenic capacity and subsequent contribution to metabolism of each localized BAT depot. Therefore, the limitations encountered in the currently available gene expression studies as well as in ^{18}FDG-PET-CT-scan-based studies underscore the necessity to devise alternate approaches to quantify and qualify BAT in humans.

In our current study, we applied an approach able to predict and quantify brown and brite adipocytes in heterogeneous human BAT biopsies by combining gene signatures common between mice and human. So far, there has been an effort to translate the genetic markers of murine brown and brite adipocytes in humans (Cypess et al., 2013; de Jong et al., 2015; Jespersen et al., 2013; Sharp et al., 2012; Wu et al., 2012); however, most of the markers from mice have failed to be informative for the presence of brown or brite adipocytes in human biopsies (de Jong et al., 2015). Exceptions are three surface markers that can distinguish between brown and brite and white adipocytes, to differentiate with a great potential between these three cell types in human biopsies, and which can be used to identify BAT in a heterogeneous sample (Ussar et al., 2014). The limitations that arise from using murine markers in human analyses result mainly from the intrinsic transcriptome differences between these two organisms (Lin et al., 2014). Moreover, the main approaches for identifying the presence of brown and brite adipocytes in human biopsies have several limitations because they are based on *Ucp1* mRNA expression, which might not adequately describe the cell composition. This was already demonstrated in a previous study, in which we could show that the presence of multilocular brown adipocytes in iWAT does not directly correlate with *Ucp1* mRNA expression (Rosenwald et al., 2013b). Furthermore, microscopic analysis of iWAT sections revealed that cold exposure induced the appearance of multilocular brown adipocytes, which persisted even after the mice returned to room temperature and disappeared only after 5 weeks of warm acclimatization, suggesting that brown adipocytes remain present in the iWAT depot, even though they are not expressing *Ucp1* (Wang et al., 2013). Thus, *Ucp1* expression probably depicts only active brown adipocytes and cannot serve as a marker for the presence of inducible brown adipocytes.

Most studies that deal with the identification of markers that can define brown, brite, and white adipocytes propose a single marker as means to quantify and qualify these cell types in a complex biopsy. As calculated for our ROCs and AUC analysis, we could show that single markers have substantially less predictive power in comparison to a support vector machine classifier consisting of multiple markers. With the deconvolution approach used in the present study, we cannot predict the actual thermogenic capacity of a biopsy but only the presence of adipocytes that have the potential to perform thermogenesis and that are the brown and brite adipocyte content. This results from the fact that we used a defining cell signature to deconvolute adipose tissue that does not contain only brown and brite but also white adipocyte markers. Thus, our algorithm can estimate the actual content of brown and brite adipocytes but does not distinguish between UCP1 and non-UCP1 thermogenic cells, due to the limited ability to purify these individual cells. The deconvolution of cell types from heterogeneous tissues has been an increasingly attractive approach to extract the cell-centered level context from bulk RNA-seq. The most recent developed tools have been mostly applied to highly heterogeneous samples, such as blood and cancer samples (Shen-Orr and Gaujoux, 2013), and thus are often specialized for investigating mixtures of immune cells. This is one of the first applications of cell deconvolution to RNA-seq-based gene expression profiles from WAT and BAT. In fact, a deconvolution study published in 2006 tried to use BAT and WAT in order to deconvolute the development of mammary glands, but the cell-type-specific gene lists used were based on microarray data (Wang et al., 2006). In addition, Cheng et al. (2018) recently devised a computational tool, which can be used to predict mouse and human adipose browning capacity based on raw gene expression data. By integrating murine BAT and WAT transcriptional profiles from 7 independent studies, they identified 59 gene markers. 16 of them (15 brown and 1 white marker) appear also in our gene marker list. This relatively limited number of overlapping gene markers reflects mainly the fact that our marker list was defined based on transcriptional profiles of pure murine brown and brite and white adipocyte populations. Regarding the computational analysis, most methods of deconvolution use either standard linear regression (Abbas et al., 2009), semi-supervised NMF algorithms (Gaujoux and Seoighe, 2013), or the quadratic programming approach, such as the DSA algorithm, which we found to be robust for both our mouse and human datasets (Zhong et al., 2013). This is demonstrated by the ability of the DSA to accurately estimate the brown percentages from the cohort 2 samples, in which the samples are complex mixtures of heterogeneous adipose tissues unlike the relatively high purity of the cohort 1 samples. Given that our validation experiments in C57BL/6 and SV129 mice in different anatomical depots, as well as on deep neck BAT samples (cohort 2), which are extremely heterogeneous and contain different proportions of white and brown and brite adipocytes, we propose the algorithm can be applied also to other tissues. One very important caveat is

the sampling technique, especially in case of large and heterogeneous fat depots, such as the abdominal subcutaneous WAT. Although samples in our study yielded large amounts of adipose tissue, in the case of thin needle biopsies, more than one biopsy from different areas might be required. Future studies will be required to calculate the heterogeneity to determine ideal sample technique and size for other depots.

Because the prominent BAT depots are more difficult to sample, mainly due to their anatomic location and small size, quantification of WAT browning is clearly the easier option, even though fat depots in the supraclavicular and neck regions possess a higher browning capacity than abdominal WAT (Ouellet et al., 2012). We have recently shown that the activation of BAT in humans follows a strictly cranio-caudal gradient, as no patient showed active BAT in the abdomen without active BAT in the mediastinum and supraclavicular area, and there were no cases with active BAT in the mediastinum without supraclavicular activation (Becker et al., 2016). Based on this observation, we hypothesize that patients with thermogenic adipocytes in the abdominal subcutaneous WAT will have more BAT also in the supraclavicular and deep neck regions; however, further studies will be necessary to determine the exact predictive value of other adipose tissue depots for whole-body brown adipocyte content.

STAR★METHODS

Detailed methods are provided in the online version of this paper and include the following:

- KEY RESOURCES TABLE
- CONTACT FOR REAGENT AND RESOURCE SHARING
- EXPERIMENTAL MODEL AND SUBJECT DETAILS
  - Mice
  - Clinical Studies
- METHOD DETAILS
  - Mature adipocyte preparation and FACS of adipocyte subpopulations
  - RNA extraction, cDNA synthesis and quantitative real-time-PCR (qPCR)
  - Murine adipocyte RNA-Seq
  - Human adipose tissue RNA-Seq
  - RNA-Seq computational analysis
  - Selection of conserved brown and white markers between mouse and human
- QUANTIFICATION AND STATISTICAL ANALYSIS
  - Deconvolution analysis
  - Support Vector Machine for classification of brown and white adipose samples
  - Measure of Brown Adipocyte Content
  - Statistical analysis
- DATA AND SOFTWARE AVAILABILITY

SUPPLEMENTAL INFORMATION

Supplemental Information includes five figures, eight tables, and one data file and can be found with this article online at https://doi.org/10.1016/j.celrep.2018.09.044.

ACKNOWLEDGMENTS

We acknowledge E. Kiehlmann for tissue microscopy, Flow Cytometry Facilities of University of Zürich and ETH Zürich for FACS, Tobias Hildebrandt and Werner Rust (BI) for their assistance with library preparation and RNA-seq, and Eric Simon (BI) for support with bioinformatics analyses. The work was in part funded by the Swiss National Foundation (C.W., 31003A_162887) and the EASD (C.W., GR).

AUTHOR CONTRIBUTIONS

A.P., G.G.L., M.B., H.N., and C.W. conceived and designed the study. A.P., G.G.L., and C.W. designed and developed the methodology. A.P., W.S., and H.D. performed mouse experiments, adipocyte FACS analysis, and adipocyte microscopy. M.B. and L.B. performed RNA extraction and RNA-seq of human samples. S.M. collected mouse mature adipocyte fraction samples and extracted RNA. N.A. performed library preparation for RNA-seq. G.G.L., N.D.P., F.F.-A., L.O., H.K., and E.S. developed the algorithm and performed the computational analysis. G.G.L. and L.O. were responsible for data availability. M.B., L.B., M.E.L., P.S., L.V., P.N., K.A.V., T.N., M.T., J.U., S.E., E.R., and G.R. provided the human material. A.P., G.G.L., M.B., H.N., and C.W. wrote the manuscript and generated the figures, with feedback from all other authors. H.N. and C.W. supervised the study.

DECLARATION OF INTERESTS

The authors declare no competing interests.

Received: March 4, 2018
Revised: August 20, 2018
Accepted: September 12, 2018
Published: October 16, 2018

REFERENCES

Abbas, A.R., Wolslegel, K., Seshasayee, D., Modrusan, Z., and Clark, H.F. (2009). Deconvolution of blood microarray data identifies cellular activation patterns in systemic lupus erythematosus. PLoS ONE *4*, e6098.

Bartesaghi, S., Hallen, S., Huang, L., Svensson, P.-A., Momo, R.A., Wallin, S., Carlsson, E.K., Forslöw, A., Seale, P., and Peng, X.-R. (2015). Thermogenic activity of UCP1 in human white fat-derived beige adipocytes. Mol. Endocrinol. *29*, 130–139.

Becker, A.S., Nagel, H.W., Wolfrum, C., and Burger, I.A. (2016). Anatomical grading for metabolic activity of brown adipose tissue. PLoS ONE *11*, e0149458.

Broeders, E.P., Nascimento, E.B., Havekes, B., Brans, B., Roumans, K.H., Tailleux, A., Schaart, G., Kouach, M., Charton, J., Deprez, B., et al. (2015). The bile acid chenodeoxycholic acid increases human brown adipose tissue activity. Cell Metab. *22*, 418–426.

Cannon, B., and Nedergaard, J. (2004). Brown adipose tissue: function and physiological significance. Physiol. Rev. *84*, 277–359.

Carey, A.L., Formosa, M.F., Van Every, B., Bertovic, D., Eikelis, N., Lambert, G.W., Kalff, V., Duffy, S.J., Cherk, M.H., and Kingwell, B.A. (2013). Ephedrine activates brown adipose tissue in lean but not obese humans. Diabetologia *56*, 147–155.

Chen, K.Y., Brychta, R.J., Linderman, J.D., Smith, S., Courville, A., Dieckmann, W., Herscovitch, P., Millo, C.M., Remaley, A., Lee, P., and Celi, F.S. (2013). Brown fat activation mediates cold-induced thermogenesis in adult humans in response to a mild decrease in ambient temperature. J. Clin. Endocrinol. Metab. *98*, E1218–E1223.

Cheng, Y., Jiang, L., Keipert, S., Zhang, S., Hauser, A., Graf, E., Strom, T., Tschöp, M., Jastroch, M., and Perocchi, F. (2018). Prediction of adipose browning capacity by systematic integration of transcriptional profiles. Cell Rep. *23*, 3112–3125.

Collins, S., Daniel, K.W., Petro, A.E., and Surwit, R.S. (1997). Strain-specific response to β 3-adrenergic receptor agonist treatment of diet-induced obesity in mice. Endocrinology *138*, 405–413.

Cousin, B., Cinti, S., Morroni, M., Raimbault, S., Ricquier, D., Pénicaud, L., and Casteilla, L. (1992). Occurrence of brown adipocytes in rat white adipose tissue: molecular and morphological characterization. J. Cell Sci. *103*, 931–942.

Cypess, A.M., Lehman, S., Williams, G., Tal, I., Rodman, D., Goldfine, A.B., Kuo, F.C., Palmer, E.L., Tseng, Y.-H., Doria, A., et al. (2009). Identification and importance of brown adipose tissue in adult humans. N. Engl. J. Med. *360*, 1509–1517.

Cypess, A.M., White, A.P., Vernochet, C., Schulz, T.J., Xue, R., Sass, C.A., Huang, T.L., Roberts-Toler, C., Weiner, L.S., Sze, C., et al. (2013). Anatomical localization, gene expression profiling and functional characterization of adult human neck brown fat. Nat. Med. *19*, 635–639.

Cypess, A.M., Weiner, L.S., Roberts-Toler, C., Franquet Elía, E., Kessler, S.H., Kahn, P.A., English, J., Chatman, K., Trauger, S.A., Doria, A., and Kolodny, G.M. (2015). Activation of human brown adipose tissue by a β3-adrenergic receptor agonist. Cell Metab. *21*, 33–38.

de Jong, J.M.A., Larsson, O., Cannon, B., and Nedergaard, J. (2015). A stringent validation of mouse adipose tissue identity markers. Am. J. Physiol. Endocrinol. Metab. *308*, E1085–E1105.

DeLuca, D.S., Levin, J.Z., Sivachenko, A., Fennell, T., Nazaire, M.D., Williams, C., Reich, M., Winckler, W., and Getz, G. (2012). RNA-SeQC: RNA-seq metrics for quality control and process optimization. Bioinformatics *28*, 1530–1532.

Dobin, A., Davis, C.A., Schlesinger, F., Drenkow, J., Zaleski, C., Jha, S., Batut, P., Chaisson, M., and Gingeras, T.R. (2013). STAR: ultrafast universal RNA-seq aligner. Bioinformatics *29*, 15–21.

Durinck, S., Moreau, Y., Kasprzyk, A., Davis, S., De Moor, B., Brazma, A., and Huber, W. (2005). BioMart and Bioconductor: a powerful link between biological databases and microarray data analysis. Bioinformatics *21*, 3439–3440.

Feldmann, H.M., Golozoubova, V., Cannon, B., and Nedergaard, J. (2009). UCP1 ablation induces obesity and abolishes diet-induced thermogenesis in mice exempt from thermal stress by living at thermoneutrality. Cell Metab. *9*, 203–209.

Frontini, A., Vitali, A., Perugini, J., Murano, I., Romiti, C., Ricquier, D., Guerrieri, M., and Cinti, S. (2013). White-to-brown transdifferentiation of omental adipocytes in patients affected by pheochromocytoma. Biochim. Biophys. Acta *1831*, 950–959.

Gaujoux, R., and Seoighe, C. (2013). CellMix: a comprehensive toolbox for gene expression deconvolution. Bioinformatics *29*, 2211–2212.

Giralt, M., and Villarroya, F. (2013). White, brown, beige/brite: different adipose cells for different functions? Endocrinology *154*, 2992–3000.

Guerra, C., Koza, R.A., Yamashita, H., Walsh, K., and Kozak, L.P. (1998). Emergence of brown adipocytes in white fat in mice is under genetic control. Effects on body weight and adiposity. J. Clin. Invest. *102*, 412–420.

Harms, M., and Seale, P. (2013). Brown and beige fat: development, function and therapeutic potential. Nat. Med. *19*, 1252–1263.

Jespersen, N.Z., Larsen, T.J., Peijs, L., Daugaard, S., Homøe, P., Loft, A., de Jong, J., Mathur, N., Cannon, B., Nedergaard, J., et al. (2013). A classical brown adipose tissue mRNA signature partly overlaps with brite in the supraclavicular region of adult humans. Cell Metab. *17*, 798–805.

Johnson, W.E., Li, C., and Rabinovic, A. (2007). Adjusting batch effects in microarray expression data using empirical Bayes methods. Biostatistics *8*, 118–127.

Kalinovich, A.V., de Jong, J.M.A., Cannon, B., and Nedergaard, J. (2017). UCP1 in adipose tissues: two steps to full browning. Biochimie *134*, 127–137.

Karatzoglou, A., Smola, A., Hornik, K., and Zeileis, A. (2004). kernlab - an S4 package for kernel methods in R. J. Stat. Softw. *11*, 1–20.

Law, C.W., Chen, Y., Shi, W., and Smyth, G.K. (2014). voom: precision weights unlock linear model analysis tools for RNA-seq read counts. Genome Biol. *15*, R29.

Lee, Y.H., Mottillo, E.P., and Granneman, J.G. (2014). Adipose tissue plasticity from WAT to BAT and in between. Biochim. Biophys. Acta *1842*, 358–369.

Leitner, B.P., Huang, S., Brychta, R.J., Duckworth, C.J., Baskin, A.S., McGehee, S., Tal, I., Dieckmann, W., Gupta, G., Kolodny, G.M., et al. (2017). Mapping of human brown adipose tissue in lean and obese young men. Proc. Natl. Acad. Sci. USA *114*, 8649–8654.

Lidell, M.E., Betz, M.J., Dahlqvist Leinhard, O., Heglind, M., Elander, L., Slawik, M., Mussack, T., Nilsson, D., Romu, T., Nuutila, P., et al. (2013). Evidence for two types of brown adipose tissue in humans. Nat. Med. *19*, 631–634.

Lim, Y.C., Chia, S.Y., Jin, S., Han, W., Ding, C., and Sun, L. (2016). Dynamic DNA methylation landscape defines brown and white cell specificity during adipogenesis. Mol. Metab. *5*, 1033–1041.

Lin, S., Lin, Y., Nery, J.R., Urich, M.A., Breschi, A., Davis, C.A., Dobin, A., Zaleski, C., Beer, M.A., Chapman, W.C., et al. (2014). Comparison of the transcriptional landscapes between human and mouse tissues. Proc. Natl. Acad. Sci. USA *111*, 17224–17229.

Müller, S., Balaz, M., Stefanicka, P., Varga, L., Amri, E.-Z., Ukropec, J., Wollscheid, B., and Wolfrum, C. (2016). Proteomic analysis of human brown adipose tissue reveals utilization of coupled and uncoupled energy expenditure pathways. Sci. Rep. *6*, 30030.

Orava, J., Nuutila, P., Lidell, M.E., Oikonen, V., Noponen, T., Viljanen, T., Scheinin, M., Taittonen, M., Niemi, T., Enerbäck, S., and Virtanen, K.A. (2011). Different metabolic responses of human brown adipose tissue to activation by cold and insulin. Cell Metab. *14*, 272–279.

Ouellet, V., Labbé, S.M., Blondin, D.P., Phoenix, S., Guérin, B., Haman, F., Turcotte, E.E., Richard, D., and Carpentier, A.C. (2012). Brown adipose tissue oxidative metabolism contributes to energy expenditure during acute cold exposure in humans. J. Clin. Invest. *122*, 545–552.

Petrovic, N., Walden, T.B., Shabalina, I.G., Timmons, J.A., Cannon, B., and Nedergaard, J. (2010). Chronic peroxisome proliferator-activated receptor γ (PPARgamma) activation of epididymally derived white adipocyte cultures reveals a population of thermogenically competent, UCP1-containing adipocytes molecularly distinct from classic brown adipocytes. J. Biol. Chem. *285*, 7153–7164.

Fan, R.-E., Chang, K.-W., Hsieh, C.-J., Wang, X.-R., and Lin, C.-J. (2008). LIBLINEAR: a library for large linear classification. J. Mach. Learn. Res. *9*, 1871–1874.

Rosenwald, M., and Wolfrum, C. (2014). The origin and definition of brite versus white and classical brown adipocytes. Adipocyte *3*, 4–9.

Rosenwald, M., Perdikari, A., Weber, E., and Wolfrum, C. (2013a). Phenotypic analysis of BAT versus WAT differentiation. Curr. Protoc. Mouse Biol. *3*, 205–216.

Rosenwald, M., Perdikari, A., Rülicke, T., and Wolfrum, C. (2013b). Bi-directional interconversion of brite and white adipocytes. Nat. Cell Biol. *15*, 659–667.

Sanchez-Gurmaches, J., and Guertin, D.A. (2014a). Adipocyte lineages: tracing back the origins of fat. Biochim. Biophys. Acta *1842*, 340–351.

Sanchez-Gurmaches, J., and Guertin, D.A. (2014b). Adipocytes arise from multiple lineages that are heterogeneously and dynamically distributed. Nat. Commun. *5*, 4099.

Schulz, T.J., Huang, T.L., Tran, T.T., Zhang, H., Townsend, K.L., Shadrach, J.L., Cerletti, M., McDougall, L.E., Giorgadze, N., Tchkonia, T., et al. (2011). Identification of inducible brown adipocyte progenitors residing in skeletal muscle and white fat. Proc. Natl. Acad. Sci. USA *108*, 143–148.

Schwalie, P.C., Dong, H., Zachara, M., Russeil, J., Alpern, D., Akchiche, N., Caprara, C., Sun, W., Schlaudraff, K.U., Soldati, G., et al. (2018). A stromal cell population that inhibits adipogenesis in mammalian fat depots. Nature *559*, 103–108.

Sharp, L.Z., Shinoda, K., Ohno, H., Scheel, D.W., Tomoda, E., Ruiz, L., Hu, H., Wang, L., Pavlova, Z., Gilsanz, V., and Kajimura, S. (2012). Human BAT possesses molecular signatures that resemble beige/brite cells. PLoS ONE *7*, e49452.

Shen-Orr, S.S., and Gaujoux, R. (2013). Computational deconvolution: extracting cell type-specific information from heterogeneous samples. Curr. Opin. Immunol. *25*, 571–578.

Shinoda, K., Luijten, I.H.N., Hasegawa, Y., Hong, H., Sonne, S.B., Kim, M., Xue, R., Chondronikola, M., Cypess, A.M., Tseng, Y.-H., et al. (2015). Genetic and functional characterization of clonally derived adult human brown adipocytes. Nat. Med. *21*, 389–394.

Stanford, K.I., Middelbeek, R.J.W., Townsend, K.L., An, D., Nygaard, E.B., Hitchcox, K.M., Markan, K.R., Nakano, K., Hirshman, M.F., Tseng, Y.-H., and Goodyear, L.J. (2013). Brown adipose tissue regulates glucose homeostasis and insulin sensitivity. J. Clin. Invest. *123*, 215–223.

Timmons, J.A., Wennmalm, K., Larsson, O., Walden, T.B., Lassmann, T., Petrovic, N., Hamilton, D.L., Gimeno, R.E., Wahlestedt, C., Baar, K., et al. (2007). Myogenic gene expression signature establishes that brown and white adipocytes originate from distinct cell lineages. Proc. Natl. Acad. Sci. USA *104*, 4401–4406.

Trapnell, C., Hendrickson, D.G., Sauvageau, M., Goff, L., Rinn, J.L., and Pachter, L. (2013). Differential analysis of gene regulation at transcript resolution with RNA-seq. Nat. Biotechnol. *31*, 46–53.

Ussar, S., Lee, K.Y., Dankel, S.N., Boucher, J., Haering, M.F., Kleinridders, A., Thomou, T., Xue, R., Macotela, Y., Cypess, A.M., et al. (2014). ASC-1, PAT2, and P2RX5 are cell surface markers for white, beige, and brown adipocytes. Sci. Transl. Med. *6*, 247ra103.

van Marken Lichtenbelt, W.D., Vanhommerig, J.W., Smulders, N.M., Drossaerts, J.M.A.F.L., Kemerink, G.J., Bouvy, N.D., Schrauwen, P., and Teule, G.J.J. (2009). Cold-activated brown adipose tissue in healthy men. N. Engl. J. Med. *360*, 1500–1508.

Virtanen, K.A., Lidell, M.E., Orava, J., Heglind, M., Westergren, R., Niemi, T., Taittonen, M., Laine, J., Savisto, N.-J., Enerbäck, S., and Nuutila, P. (2009). Functional brown adipose tissue in healthy adults. N. Engl. J. Med. *360*, 1518–1525.

Waldén, T.B., Hansen, I.R., Timmons, J.A., Cannon, B., and Nedergaard, J. (2012). Recruited vs. nonrecruited molecular signatures of brown, "brite," and white adipose tissues. Am. J. Physiol. Endocrinol. Metab. *302*, E19–E31.

Wang, M., Master, S.R., and Chodosh, L.A. (2006). Computational expression deconvolution in a complex mammalian organ. BMC Bioinformatics *7*, 328.

Wang, Q.A., Tao, C., Gupta, R.K., and Scherer, P.E. (2013). Tracking adipogenesis during white adipose tissue development, expansion and regeneration. Nat. Med. *19*, 1338–1344.

Wang, W., Kissig, M., Rajakumari, S., Huang, L., Lim, H.W., Won, K.J., and Seale, P. (2014). Ebf2 is a selective marker of brown and beige adipogenic precursor cells. Proc. Natl. Acad. Sci. USA *111*, 14466–14471.

Wang, H., Liu, L., Lin, J.Z., Aprahamian, T.R., and Farmer, S.R. (2016). Browning of white adipose tissue with roscovitine induces a distinct population of UCP1^{+} adipocytes. Cell Metab. *24*, 835–847.

Whittle, A.J., Carobbio, S., Martins, L., Slawik, M., Hondares, E., Vázquez, M.J., Morgan, D., Csikasz, R.I., Gallego, R., Rodriguez-Cuenca, S., et al. (2012). BMP8B increases brown adipose tissue thermogenesis through both central and peripheral actions. Cell *149*, 871–885.

Wu, J., Boström, P., Sparks, L.M., Ye, L., Choi, J.H., Giang, A.-H., Khandekar, M., Virtanen, K.A., Nuutila, P., Schaart, G., et al. (2012). Beige adipocytes are a distinct type of thermogenic fat cell in mouse and human. Cell *150*, 366–376.

Young, P., Arch, J.R.S., and Ashwell, M. (1984). Brown adipose tissue in the parametrial fat pad of the mouse. FEBS Lett. *167*, 10–14.

Zhong, Y., Wan, Y.W., Pang, K., Chow, L.M., and Liu, Z. (2013). Digital sorting of complex tissues for cell type-specific gene expression profiles. BMC Bioinformatics *14*, 89.

STAR★METHODS

KEY RESOURCES TABLE

REAGENT or RESOURCE	SOURCE	IDENTIFIER
Chemicals, Peptides, and Recombinant Proteins		
Trizol reagent	Invitrogen	Cat# 15596026
DNase I (RNase-free)	NEB	Cat# M0303
Fast SYBR green Master Mix	ThermoFisher	Cat# 4385612
Pellet Paint Co-Precipitant	Merck-Millipore	Cat# 69049
Agilent RNA 6000 Nano Kit	Agilent	Cat# 5067-1511
Agilent RNA 6000 Pico Kit	Agilent	Cat# 5067-1513
Ethanol	Sigma-Aldrich	Cat# E7023
PBS	GIBCO	Cat# 10010023
Paraformaldehyde	Sigma-Aldrich	Cat# P6148
Critical Commercial Assays		
High Capacity cDNA RT kit	Applied Biosystems	Cat# 4368814
RNeasy plus Micro Kit	QIAGEN	Cat# 74034
RNeasy Lipid Tissue Mini Kit	QIAGEN	Cat# 74804
TruSeq RNA library prep kit	Illumina	Cat# RS-122-2301
SMART-Seq v4 Ultra Low Input RNA Kit	Clontech	Cat# 634891
Ovation Single Cell RNaseq system	NuGEN	Cat# 0342-32
Deposited Data		
RNA sequencing data	European Nucleotide Archive	PRJEB20634
BATLAS webtool	This paper	https://shiny.hest.ethz.ch/BATLAS/
Experimental Models: Organisms/Strains		
Ucp1-eGFP mice	Christian Wolfrum	Rosenwald et al., 2013b
C57BL/6 mice	Charles River	C57BL/6NCrl Strain code 027
129/SV mice	Charles River	129S2/SvPasCrl Strain code 287
Oligonucleotides		
qPCR primers	Microsynth	Sequences are listed in Table S8
Software and Algorithms		
GraphPad Prism 7	GraphPad software	version 7.03
ViiA7 software	Applied Biosystems	version 1.2.3
STAR v2.4.0j	Dobin et al., 2013	N/A
Picard Tools suite	Broad Institute MIT	N/A
Cufflinks	Trapnell et al., 2013	version 2.2.1
RNASeQC	DeLuca et al., 2012	version 1.18
Bioconductor LIMMA analysis R package	Law et al., 2014	N/A
BioMart and Bioconductor	Durinck et al., 2005	N/A
CellMix package	Gaujoux and Seoighe, 2013	N/A
R package kernlab	Karatzoglou et al., 2004	N/A
Other		
Agilent 2100 Bioanalyzer	Agilent	N/A
Agilent 2200 TapeStation	Agilent	N/A
Illumina HiSeq2000 system	Illumina	N/A
Illumina HiSeq2500 system	Illumina	N/A
Aria III high-speed sorter	BD Bioscience	N/A

CONTACT FOR REAGENT AND RESOURCE SHARING

Further information and requests for resources and reagents should be directed to and will be fulfilled by the Lead Contact, Professor Christian Wolfrum (christian-wolfrum@ethz.ch).

EXPERIMENTAL MODEL AND SUBJECT DETAILS

Mice

C57BL/6N wild-type mice for experiments and breeding of transgenic lines were obtained from Charles River. The *Ucp1-GFP* mouse used was described previously (Rosenwald et al., 2013b). All experiments were performed with adult (13-15 weeks) male or female mice kept on an inverted 12 h dark/light cycle, fed *ad libitum* chow diet. For the cold stimulation, animals were housed in type II cages with two animals per cage, 30 g of bedding and one plastic house in a custom-made temperature-controlled Phenomaster (TSE Systems) at an air flow of 0.5 $l.min^{-1}$. Following acclimatization at 23 °C, air temperature was lowered to 8 °C for 7 days. For tissue sampling, animals were euthanized singly in a carbon dioxide atmosphere. Popliteal lymph nodes were carefully removed from iWAT depots for cellular separations and gene expression analysis. All animal procedures were approved by the Veterinary office of the Canton of Zürich.

Clinical Studies

Cohort 1

The clinical study for cohort 1 was approved by the Ethics Committee of the Hospital District of Southwest Finland and conducted according to the principles of the Declaration of Helsinki. All study participants provided written consent prior to entering the study. The subjects were screened for medical history and status, and only healthy volunteers were enrolled in the study. PET-CT scan and tissue biopsies were performed as described in the previous publication (Orava et al., 2011). Briefly, the subjects underwent a PET-CT examination after an overnight fast. On the cold exposure day, the subjects spent 2 hours wearing light clothing in a room with an ambient temperature of 17 ± 1°C before moving into the PET-CT room, which had an air temperature of 23°C. During the PET-CT session, one foot of the subject was placed intermittently (5 min in/5 min out) in cold water at a temperature of 8 ± 1°C. Detailed description of PET-CT examination is available in (Orava et al., 2011). The site of the biopsy was selected based on the cold exposure ^{18}FDG-PET-CT image that showed activated BAT. A subcutaneous WAT sample was collected from the same incision. The biopsies were obtained under local lidocaine-epinephrine anesthesia by a plastic surgeon at normal room temperature (20°C) one week after the PET-CT examination. Immediately after removal, the tissue samples were snap-frozen in liquid nitrogen and stored at −80°C.

Cohort 2

The clinical study for cohort 2 was approved by the Local Ethics Committee (University Hospital in Bratislava, Slovakia) and it conforms to the ethical guidelines of the 2000 Helsinki declaration. All study participants provided witnessed written informed consent prior to entering the study. Deep neck and adjacent subcutaneous adipose tissue samples were obtained from the lower third of the neck by an experienced ENT surgeon from 18 individuals (1 Male/ 17 Female) during neck surgery under general anesthesia, age between 22 to 73 years old and BMI between 19 to 34 kg/m^2 (Table S7). The deep neck adipose tissue sample was taken from pre- and paravertebral space between the common carotid and trachea in case of thyroid surgery and just laterally to the carotid sheath in case of branchial cleft cyst surgery. In all cases, the surgical approach was sufficient to reach and sample the deep neck adipose tissue without any additional morbidity. Patients with malignant disease and subjects younger than 18 years were excluded from participation in the study. Adipose tissue samples were immediately cleaned from blood and connective tissue, and frozen in liquid nitrogen until further processing. The clinical study on obese subjects (20/42 Male/Female; age 40.5 ± 1.6 years; BMI 41.2 ± 0.9 kg/m^2) undergoing caloric restriction with a daily intake of 800 kcal was approved by the ethics committee at the University Hospital of Heidelberg, Germany (S-365/2007). It conforms to the ethical guidelines of the 2000 Helsinki declaration. All participants provided witnessed written informed consent prior to entering the study. The study was registered as NCT00773565.

METHOD DETAILS

Mature adipocyte preparation and FACS of adipocyte subpopulations

Mature adipocyte fraction isolation and FACS of adipocyte populations were performed as described previously (Rosenwald et al., 2013a). Briefly, cell sorting of adipocytes was performed using an Aria III high-speed sorter (BD Bioscience). A nozzle of 130 mm diameter, sheath pressure of 10 psi and a standard 4-way purity mask as described in the sorter manual was used during all sorts. Transgenic *Ucp1*-eGFP mice, expressing the eGFP protein under the control of *Ucp1* promoter, were cold acclimated at 8°C for 7 days and the mature adipocyte fractions from iBAT and iWAT were separated by FACS using eGFP. The adipocyte population was first defined in the forward and side scatter by size and internal complexity characteristics. The GFP^+ population was defined in the respective gate and the mature brown adipocytes were isolated from the mature fraction of iBAT. The same strategy was applied for the mature adipocyte fraction of iWAT to isolate the GFP^+ population, which constitutes brite adipocytes, and the adjacent GFP^- population that constitutes white adipocytes. For each sample, 3 or 6 same gender mice were pooled per sample and 500-3000 cells were collected directly in RNA Lysis Buffer (QIAGEN) and kept on ice until stored at −80°C.

RNA extraction, cDNA synthesis and quantitative real-time-PCR (qPCR)

RNA from FACS isolated mature adipocytes was performed with the RNeasy plus Micro Kit (QIAGEN). Total RNA was extracted from whole adipose tissues using Trizol reagent (Invitrogen) according to the manufacturer's instructions. The RNA from Cohort 1 was isolated using the RNeasy Lipid Tissue Mini Kit (QIAGEN), according to the manufacturer's protocol including the DNase treatment step. Final RNA samples were re-precipitated with NaOAc and ethanol and washed with 70% ethanol before analysis on a Nanodrop-2000 spectrophotometer. Quantitative real-time PCR was performed on Viia7 (Applied Biosystems) using SYBR green and specific primer pairs (sequences are listed in Table S8).

Murine adipocyte RNA-Seq

For both murine adipocyte RNA-Seq analyses, RNA quality was verified using the Bioanalyzer 2100 (Agilent). The cDNA libraries for RNA-Seq batch 1 and 3 were prepared using 1.2 ng total RNA input with the SMART-Seq v4 Ultra Low Input RNA Kit for RNA-Seq (Clontech). RNA-Seq was performed as 100 bp single reads on an Illumina High Seq 2500. The cDNA libraries for the RNA-Seq batch 2 were prepared using 25 ng total RNA input with the TrueSeq RNA Sample Prep Kit v2 (Illumina). RNA-Seq was performed as 50 bp single reads on an Illumina HiSeq2000. For all RNA-Seq analyses, approximately 10–30 million reads per sample were obtained.

Human adipose tissue RNA-Seq

For the cohort 1 samples, RNA-Seq libraries were prepared from 10 ng of total RNA input (RIN 6.5-8.8) with the Ovation Single Cell RNA-seq system (NuGEN) according to manufacturer's instructions. Quality and concentration of NGS libraries were verified using the Agilent 2200 TapeStation system as well as by qPCR. Barcoded libraries were pooled (8 samples per lane) and sequenced using Illumina HiSeq, obtaining > 10 million reads for each sample. For the Cohort 2 samples (deep neck BAT and subcutaneous WAT), RNA-Seq libraries were prepared using 25 ng of total RNA input with the TrueSeq RNA Sample Prep Kit v2 (Illumina) producing an average 275 bp fragment including adapters. In the final step before RNA-Seq, eight individual libraries were normalized and pooled together using the adaptor indices supplied by the manufacturer. RNA-Seq was performed as 50 bp, single reads and 7 bases index read on an Illumina HiSeq2000 instrument. Approximately 20–30 million reads per sample were obtained.

RNA-Seq computational analysis

Illumina reads were converted to the industry standard FASTQ format and aligned to the mouse and human reference genomes from Ensembl 70 using the STAR v2.4.0j program on default settings (Dobin et al., 2013). For increased alignment accuracy, the STAR genome index was generated to include splice junction annotations with the options '—sjdbGTFfile' and '—sjdbOverhang 49'. The SAM output from the STAR aligner was converted to BAM format using the Picard tools suite (Broad Institute MIT). For FPKM gene expression estimation and read counts, the programs Cufflinks version 2.2.1 was used with the following options '-u —max-bundle-frags 100000000 —no-effective-length-correction —compatible-hits-norm'(Trapnell et al., 2013) in combination with gene annotations from Ensembl 70. The quality of the RNA-Seq samples was verified with RNASeQC version 1.18 (DeLuca et al., 2012). The FPKM values of the three mouse RNA-Seq batches were merged into one gene expression table and corrected using ComBat batch correction method (Johnson et al., 2007). Differential expression analysis was performed with the uniquely mapping read counts as input for the Bioconductor LIMMA analysis R package with voom normalization (Law et al., 2014). In the case of the mouse RNA-Seq batches, the batch number was used as a factor in the LIMMA linear regression model. Genes were filtered for significant differential expression using an adjusted P values cutoff at 0.05 (after Benjamini–Hochberg multiple testing correction) and a log2 fold change of > = |0.5|.

Selection of conserved brown and white markers between mouse and human

The list of genes filtered from the different gene expression results for both mouse and human were conservatively mapped between the two species using the strict Ensembl BioMart one-to-one homology gene mapping associations (Ensembl v76) (Durinck et al., 2005). The brown and white markers were separated by fold change direction so that positive fold changes were made into a brown marker list and negative fold changes were made into white marker list. The markers genes in mouse and human were ranked by the order of their adjusted P values respectively, and genes with low expression of RPKM < 10 were excluded from the lists.

QUANTIFICATION AND STATISTICAL ANALYSIS

Deconvolution analysis

Deconvolution analysis was done using the CellMix package with all algorithms set to default parameters (Gaujoux and Seoighe, 2013). The *in silico* test set was generated from mixing different proportions of RNA-Seq reads from a pure brown adipocyte mouse sample with a pure white adipocyte mouse sample using the ratios of 1:99, 5:95,10:90, 20:80, 30:70, 40:60, 50:50, 60:40, 70:30, 80:20, 90:10 and 99:1, respectively. The estimated proportions for the test set of brown and white RNA sequenced FACS isolated mature adipocytes were compared to the actual brown adipocyte content of each sample as defined by RPKMs of *Ucp1*. In the test and validation sets, the estimated brown adipocyte proportions per sample were evaluated against the known admixture proportions of brown: white using the root mean squared error (RMSE). The Pearson product-moment correlation coefficient of each marker's gene expression values to the brown adipocyte percentages was calculated and used to rank the markers.

Support Vector Machine for classification of brown and white adipose samples

The C-constant of the regularization and sigma parameters of the radial SVC were selected through minimization of the accuracy rate in 20 independent random subsampling cross-validation stages. The R package kernlab was used to fit the SVC models (Karatzoglou et al., 2004). The different proportion of white and brown tissue samples was taken into account in the generation of the predictive models. The SVC models were trained with the 119 genes from our combined list as the features used for classification on the human and mouse datasets. The human datasets were composed of patient cohorts 1 and 2, along with a cohort of patients from our collaborators in Ulm. The mouse datasets were composed of the three batches of mature adipocytes fractions from FACS and mouse strains SV129 and C57BL6.

Measure of Brown Adipocyte Content

Paraffin Sections from adipose tissue depots of mice and from human biopsies were prepared as described previously (Rosenwald et al., 2013b), and pictures were analyzed with Cell Profiler. Adipose tissues were excised, fixed in fresh 4% paraformaldehyde (Sigma-Aldrich) in PBS (GIBCO) at pH 7.4 for 2 h at 4 °C, and cryopreserved for 30 h in 30% sucrose in PBS. The samples were flash-frozen on dry ice and stored at −80 °C. Tissues were cut at −35 °C on an HM 500 O microtome (Microm) at 50 μm thickness, mounted on Superfrost slides (Medite) and thawed at 4 °C in the dark. Sections were washed overnight in PBS at room temperature, stained in PBS + 300 nM DAPI and washed in PBS twice. Slides were embedded in VectashieldHardSet (Reactolab) and imaged on the same day. Fluorescence micrographs were acquired on an SP2 confocal microscope (Leica). To quantify the relative amount of cells, the cell morphology of at least 400 cells was assessed from different tissue planes of each sample. Cells containing only one big lipid droplet were counted as a white, whereas cells with more than 4 small lipid droplets were counted as a brite/brown adipocyte. The counting was performed in a blinded fashion. The brown adipocyte content was correlated with the actual number of multilocular adipocytes that was counted from sections of each iWAT sample.

Statistical analysis

For *in vivo* studies, littermates were randomly assigned to groups. Sample sizes were determined on the basis of previous experiments using similar methodologies. The animal numbers used for all experiments are indicated in the corresponding figure legends. All animals and human subjects were included in the statistical analyses, and the investigators were not blinded. Results are reported as mean ± SEM or SD, as indicated in the figure legends. Two-tailed unpaired Student's t test was applied on comparison of two groups. For correlation analyses Pearson's correlation coefficient was calculated. Statistical differences are indicated as * for $p < 0.05$, ** for $p < 0.01$ and *** for $p < 0.001$.

DATA AND SOFTWARE AVAILABILITY

The accession number for the RNA-seq data from mouse and human studies reported in this paper is The European Nucleotide Archive: PRJEB20634. The algorithm developed in this work can be accessed at https://shiny.hest.ethz.ch/BATLAS/.